ACSNANO

www.acsnano.org

ARTICLE

High-Speed Production of Crystalline Semiconducting Polymer Line Arrays by Meniscus Oscillation Self-Assembly

Jisoo Jeon,[#] Alvin T. L. Tan,[#] Jaeyong Lee, Jeong Eun Park, Sukyoung Won, Sanha Kim, Mostafa Bedewy, Jamison Go, Jin Kon Kim, A. John Hart,* and Jeong Jae Wie*

Cite This: https://dx.doi.org/10.1021/acsnano.0c07268

Read Online

ACCESS | Metrics & More | Article Recommendations | Supporting Information

ABSTRACT: Evaporative self-assembly of semiconducting polymers is a low-cost route to fabricating micrometer and nanoscale features for use in organic and flexible electronic devices. However, in most cases, rate is limited by the kinetics of solvent evaporation, and it is challenging to achieve uniformity over length- and time-scales that are compelling for manufacturing scale-up. In this study, we report high-throughput, continuous printing of poly(3-hexylthiophene) (P3HT) by a modified doctor blading technique with oscillatory meniscus motion—meniscus-oscillated self-assembly (MOSA), which forms P3HT features ~100 times faster than previously reported techniques. The meniscus is pinned to a roller, and the oscillatory meniscus motion of the roller generates repetitive cycles of contact-line formation and subsequent slip. The printed P3HT lines demonstrate reproducible and tailorable structures: nanometer scale thickness, micrometer scale width, submillimeter pattern intervals, and millimeter-to-centimeter scale coverage with highly defined boundaries. The line width as well as interval of P3HT patterns can be independently controlled by varying the polymer concentration levels and the rotation rate of the roller. Furthermore, grazing incidence wide-angle X-ray scattering (GIWAXS) reveals that this dynamic meniscus control technique dramatically enhances the crystallinity of P3HT. The MOSA process can potentially be applied to other geometries, and to a wide range of solution-based precursors, and therefore will develop for practical applications in printed electronics.

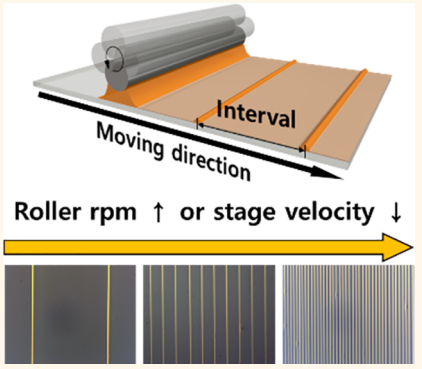

KEYWORDS: *semiconducting polymers, P3HT, self-assembly, evaporative assembly, capillary force, micropatterning*

Semiconducting polymers have drawn great attention for use in printed electronics due to their solution processability, targeting various applications including field-effect transistors, photovoltaics, displays, electronic skin, and biomedical devices.[1−4] The electronic performance of printed semiconducting polymers is mainly dependent on their crystalline order, which results in effective charge transfer. Hence, crystal engineering is a challenging yet important task for polymer-based printable electronics. Evaporative self-assembly of semiconducting polymers has been widely investigated[5−13] for facile and low-cost construction of periodically arranged nanometer scale architectures. This bottom-up approach, however, is often time-consuming and limited to achieve uniform self-assembly over large areas with high precision. To accelerate the evaporative self-assembly process, kinetic-assisted blade-casting techniques have been reported.[5,14,15] At a fixed gap between the blade and substrate, polymeric solutions develop a pinned contact line at the liquid−solid interface. The subsequent movement of the substrate causes depinning of this contact line. Repeating this controlled stick−slip phenomenon generates periodic line patterns. In addition, various curved-on-flat geometries have been used to guide evaporative assembly of polymeric solutions in order to create hierarchical structures.[16−20] However, the dwell time for contact line formation is a rate-limiting step, which limits throughput. To our knowledge, previous studies have shown evaporative assembly to take at least a few hours to pattern periodic polymer lines[21,22] and conductive nanoparticle lines[23] over centimeter scales.

Moreover, molecular self-assembly of polymers into macroscopic crystals is challenging due to the entropic penalty and broad free energy landscape for rearrangement of chain

Received: August 29, 2020
Accepted: November 20, 2020

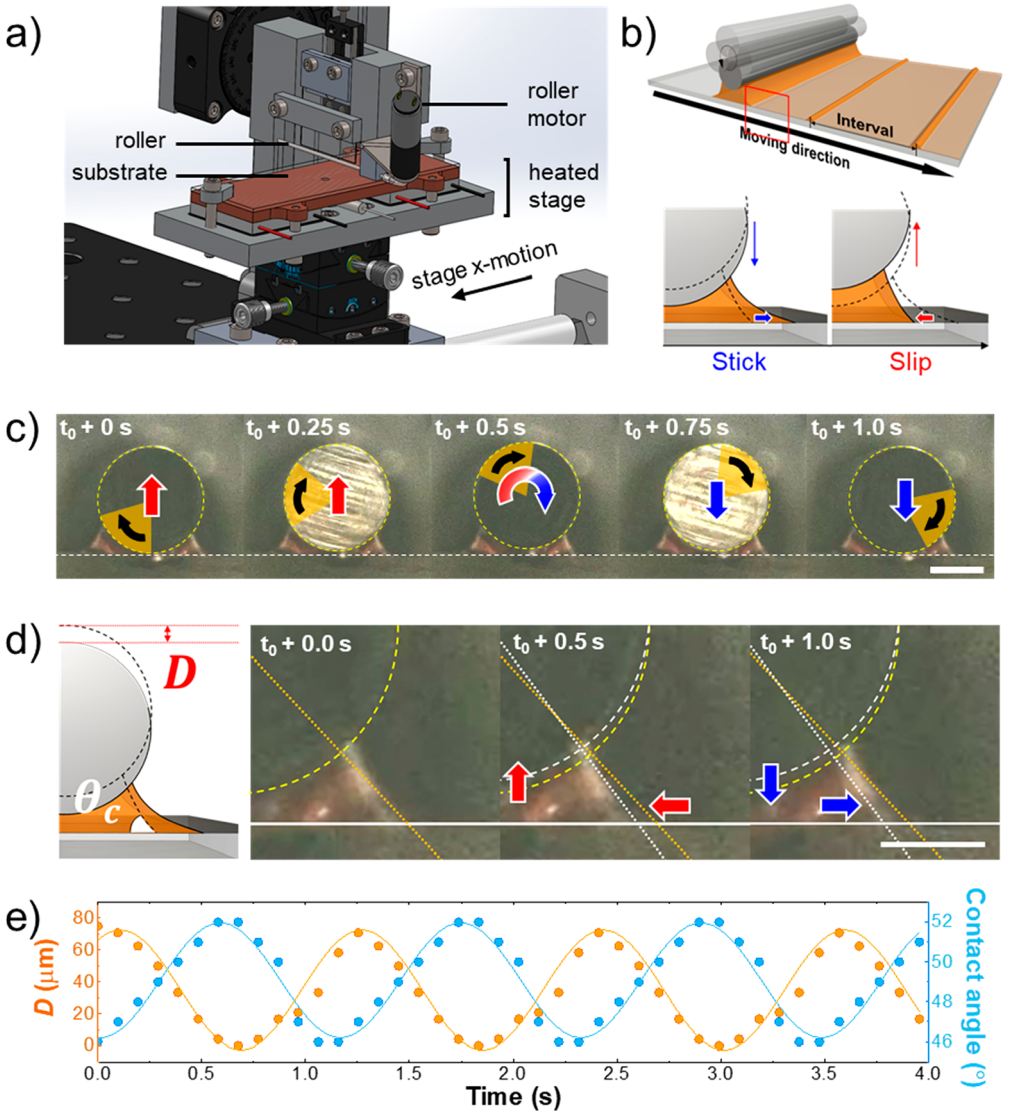

Figure 1. MOSA process and mechanism of periodic P3HT line creation. (a) Schematic illustration of custom mechanism with rotating, oscillating roller. (b) 3D schematic illustration of P3HT line pattern formation. (c) Side view optical images of roller rotation with oscillation; rotation speed, 50 rpm; scale bar, 1 mm. (d) Schematic illustration of contact angle (θ_c) and distance to the highest height of roller top (D), and contact line shift through each rotation; rotation speed, 50 rpm; scale bar, 0.5 mm. (e) The graph showing the relative position of the apex of the roller (D = 0) relative to its maximum position, and contact angle (θ_c) over time; rotation speed, 50 rpm.

conformation.[24] Thus, highly ordered regioregular polymers are advantageous for self-assembly, and molecular weight and solvent quality are also known to have a significant impact on crystallization kinetics.[24,25] The highly ordered regioregular semiconducting polymer, poly(3-hexylthiophene) (P3HT) has been extensively studied for molecular self-assembly in addition to photovoltaic applications. When P3HT crystallites are dissolved in organic solvents, amorphous P3HT segments diffuse through Brownian motion. Vicinal thiophene molecules of P3HT are drawn to each other by directional secondary intermolecular forces, edge-on $\pi-\pi$ stacking.[26−32] However, $\pi-\pi$ stacking induced molecular self-assembly is based on short-range interactions driven by diffusion limited aggregation where crystal size and speed of process are limited. Shear-induced crystallization can accelerate this process by stretching the P3HT molecules.[25] Shear alignment increases the probability for thiophene molecules to generate $\pi-\pi$ stacked crystals. As a result, long-range ordered P3HT crystals have been achieved by a rheometer through several hours of steady or dynamic oscillatory shear experiments with P3HT 2-ethylnaphthalene solution. While the Brownian motion is still dominant, shear-induced crystallization is important for creating microscale fibers of P3HT crystallites through the removal of imperfect crystal defects.

Herein, we report a continuous printing technique that utilizes oscillatory meniscus motion to regulate the width, height, and interval of hierarchically self-assembled patterns of semiconducting polymers suitable for high throughput printed electronics. To remove crystal defects, we apply rotational shear with a roller, while *in situ* evaporation of solvent occurs during shear-induced crystallization. We consider both thermodynamic and kinetic variables including P3HT concentration, temperature of the printing substrate, rotation rate of the roller, and stage velocity. On the basis of these parameter studies, we discuss the mechanism and critical parameters governing the dimensions of self-assembled P3HT crystallites as well as the role of the roller in this meniscus-oscillated self-assembly (MOSA) process.

https://dx.doi.org/10.1021/acsnano.0c07268
ACS Nano XXXX, XXX, XXX−XXX

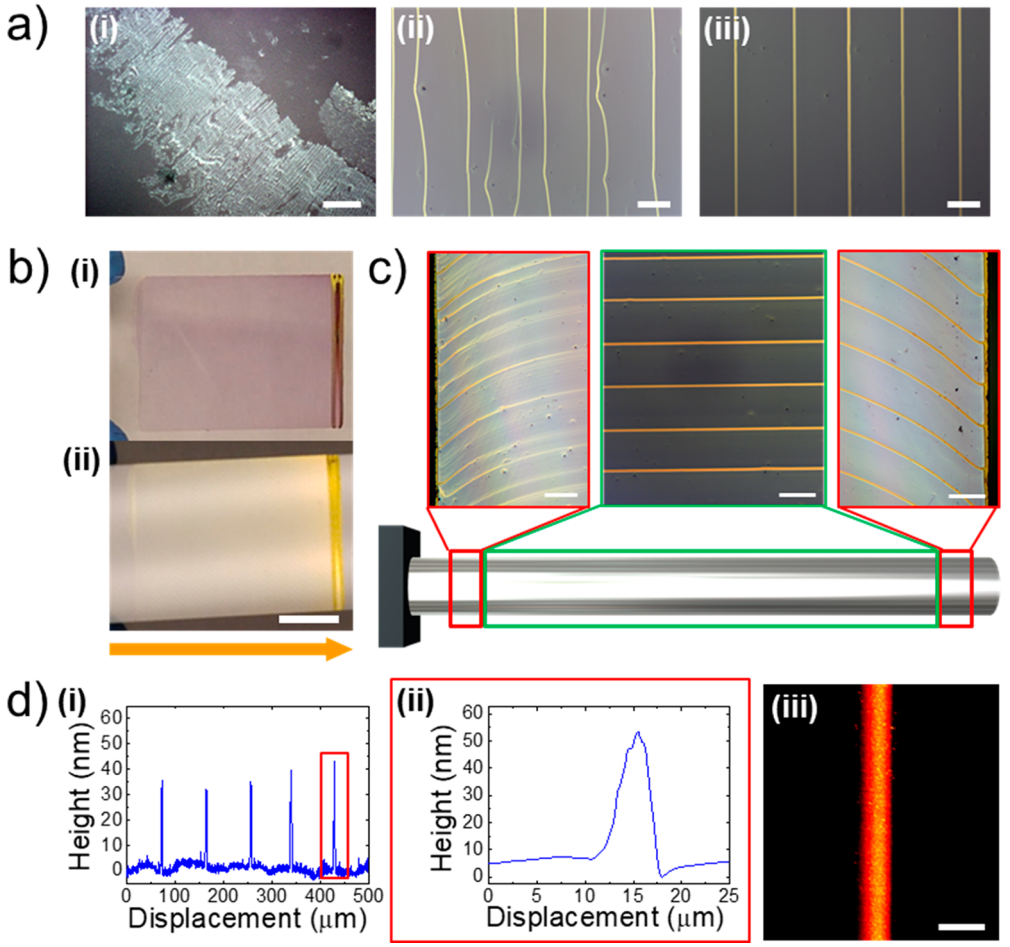

Figure 2. (a) Optical micrographs of P3HT crystallization on glass slides; scale bar, 50 μm; (i) ambient condition (25 °C stage, 1 mg/mL P3HT in toluene; rotation speed, 1250 rpm; stage speed, 1 mm/s); (ii) no rotation of roller (50 °C stage, 1 mg/mL P3HT in toluene; stage speed, 0.5 mm/s); (iii) patterning with heated stage and roller rotation (50 °C stage, 1 mg/mL P3HT in toluene; rotation speed, 1250 rpm; stage speed, 1.0 mm/s). (b) Digital images of P3HT line patterned slide glass on different light source; scale bar, 1 cm (50 °C stage, 5 mg/mL P3HT in toluene; rotation speed, 1250 rpm; stage speed, 1.0 mm/s). (c) Curved P3HT lines at roller edge due to the surface tension; scale bar, 50 μm (50 °C stage, 1 mg/mL P3HT in toluene; rotation speed, 1000 rpm; stage speed, 1.0 mm/s). (d) Height profile of P3HT line pattern (i), profilometer (ii), and (iii) AFM; scale bar, 10 μm.

RESULTS AND DISCUSSION

The design principle that enables continuous, high-speed production by MOSA involves oscillating the meniscus of an evaporating solution in contact against the deposition substrate, and enabling this high rate oscillation to be tunable. In this study, highly regioregular (>96%) P3HT with molecular weight (M_w) of 69 kDa was employed as a model system to investigate the printability of conducting polymers with MOSA. First, P3HT was dissolved in toluene at concentrations ranging from 0.5 to 5 mg/mL, at 90 °C for 1 h. As the solubility limit for P3HT is 7.54 mg/mL in toluene,[33] the maximum P3HT concentration investigated in this study was 5 mg/mL. We varied the concentration of P3HT solution up to 5 mg/mL in order to establish a stable processing time window because P3HT solution rapidly gelated at concentrations above 5 mg/mL. After complete melting and dissolution of pre-existing crystallites in $\pi-\pi$ stacked thiophene groups, the disordered amorphous P3HT solutions displayed bright-orange color due to solvatochromism.[34] A schematic for the custom-made MOSA apparatus is described in Figure 1a and Supporting Information, Figure S1a. The apparatus consists of a temperature-controlled sample stage mounted on a linear stage actuator and a roller suspended above the stage by an H-frame. The sample stage is movable in the horizontal (x-axis) direction and the position of the roller is adjustable along the vertical (y-axis) direction independent of each other. Separately, a DC motor drives the rotation of the roller, and runout in the bearing assembly for the supported end of the roller causes a repetitive periodic vertical motion with each rotation, which was measured to be approximately 71 μm. In each experiment, glass substrates were mounted onto the sample stage and the initial gap between the roller and the substrate was regulated to be 254 μm (0.01 in.) using a vertical stage micrometer (Supporting Information, Figure S1a and S1b). A small amount (20 μL) of P3HT solution was then dispensed at the roller, causing the P3HT solution to form a meniscus between the roller and the substrate, as shown in Figures 1b–d. Immediately following this step, the motion of the stage and rotation of the roller was initiated to oscillate the meniscus (Supporting Information, Figure S1c).

The evaporation of toluene initiates at the liquid–air interface as air interface causes the surface of the solvent to have weaker solvent–solvent cohesion.[35] Hence, the local P3HT concentration increases at the liquid–air interface as solvent evaporation proceeds. The polymeric solution has

https://dx.doi.org/10.1021/acsnano.0c07268
ACS Nano XXXX, XXX, XXX–XXX

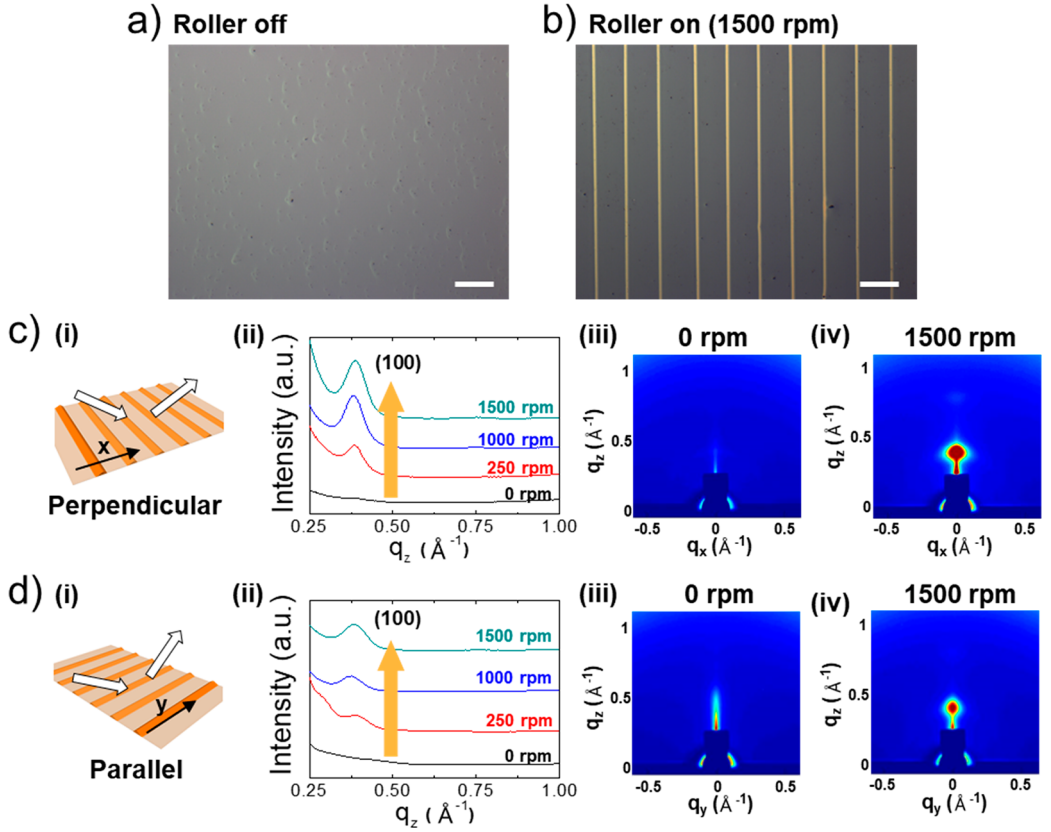

Figure 3. (a) Optical micrograph of the glass surface after assembly without rotating the roller (50 °C stage, 1 mg/mL P3Ht in toluene; stage speed, 1.0 mm/s; scale bar, 50 μm). (b) Optical micrograph of the printed P3HT line patterns by MOSA at 1500 rpm (50 °C stage, 1 mg/mL P3HT in toluene; stage speed, 0.5 mm/s; scale bar, 50 μm). (c) Grazing-incidence wide-angle X-ray scattering (GIWAXS) of the P3HT crystals for beam direction ⊥ P3HT line: (i) schematic illustration of perpendicular beam direction to P3HT line patterns; (ii) out-of-plane scattering intensity increased as roller speed increased, 2D GIWAXS patterns with roller rotation rate of (iii) 0 rpm and (iv) 1500 rpm. (d) GIWAXS of the P3HT crystals for beam direction ∥ P3HT line: (i) schematic illustration of parallel beam direction to P3HT line patterns; (ii) in-plane scattering intensity increased as roller speed increased, 2D GIWAXS patterns with roller rotation rate of (iii) 0 rpm, and (iv) 1500 rpm.

reduced interspace between the polymer segments at a higher polymer concentration, resulting in the crystallization of P3HT *via* edge-on $\pi-\pi$ stacking among vicinal thiophene chains. As described in Figure 1b–d, the P3HT solution forms a meniscus at the roller–solution interface and the substrate–solution interface. At the substrate–toluene–air interface, P3HT solution forms a contact line at angle, θ_c (Figure 1d). The eccentric rotation of the roller modulates the *y*-axis position of the meniscus by approximately 71 μm with each rotation (Supporting Information, Figure S2). The downward movement of the roller pushes the meniscus, resulting in the reduction of θ_c to 46°. Conversely, upward roller motion pulls the solution and the θ_c increases to 52° (Figure 1e). As the substrate advances and the roller oscillates, the contact line of the meniscus experiences repetition of advancing and receding motions (Figure 1b). This advancing motion generates a stick phenomenon with temporal holding of the contact line. Following this, a receding motion generates slip motion by switching the contact line opposite to the printing direction.

This oscillatory meniscus motion induces repetitive stick–slip for the P3HT solution during simultaneous *x*-axis movement of the sample stage (Figure 1e). Here, we hypothesized that the spatial interval between P3HT contact lines was determined by the temporal interval between each rotation of the roller in conjunction with the *x*-axis velocity of the stage movement.

Effects of the stage temperature, stage speed, as well as the rotation rate of the roller are crucial to a uniform printing of P3HT. The stage speed and rotation rate of roller were varied from 0.1–5 mm/s and 0–1500 rpm, respectively. When the 1 mg/mL P3HT solution was printed on a glass slide at 25 °C with 1250 rpm roller rotation and 1 mm/s stage speed, the evaporation rate of toluene was insufficient for shear-induced crystallization of P3HT *via* $\pi-\pi$ stacking as shown in Figure 2a-i and Supporting Information, S3a. In a dilute solution, intermolecular distance between P3HT coils was so large that P3HT molecules were not capable of arranging into periodic hierarchical structures. To reduce the intermolecular distance on a short time scale, we elevated the stage temperature which would increase the solvent evaporation rate and result in the evaporative self-assembly of the P3HT molecules during the high speed MOSA process. When the stage temperature was elevated to 50 °C and stage speed was reduced to 0.5 mm/s with the stationary roller, P3HT crystals were printed into line patterns as evident in Figure 2a-ii. However, kinetic effects in and of themselves are insufficient for the stationary roller system to generate periodic and uniform patterns, and the line patterns become curvilinear and irregular. Additionally, the stage speed of 1 mm/s with 1 mg/mL P3HT in toluene is still too fast to provide enough time for crystallization of P3HT into regular line patterns without a roller rotation (Supporting Information, Figure S6a-i). In the case of *in situ* rotation of the

https://dx.doi.org/10.1021/acsnano.0c07268
ACS Nano XXXX, XXX, XXX–XXX

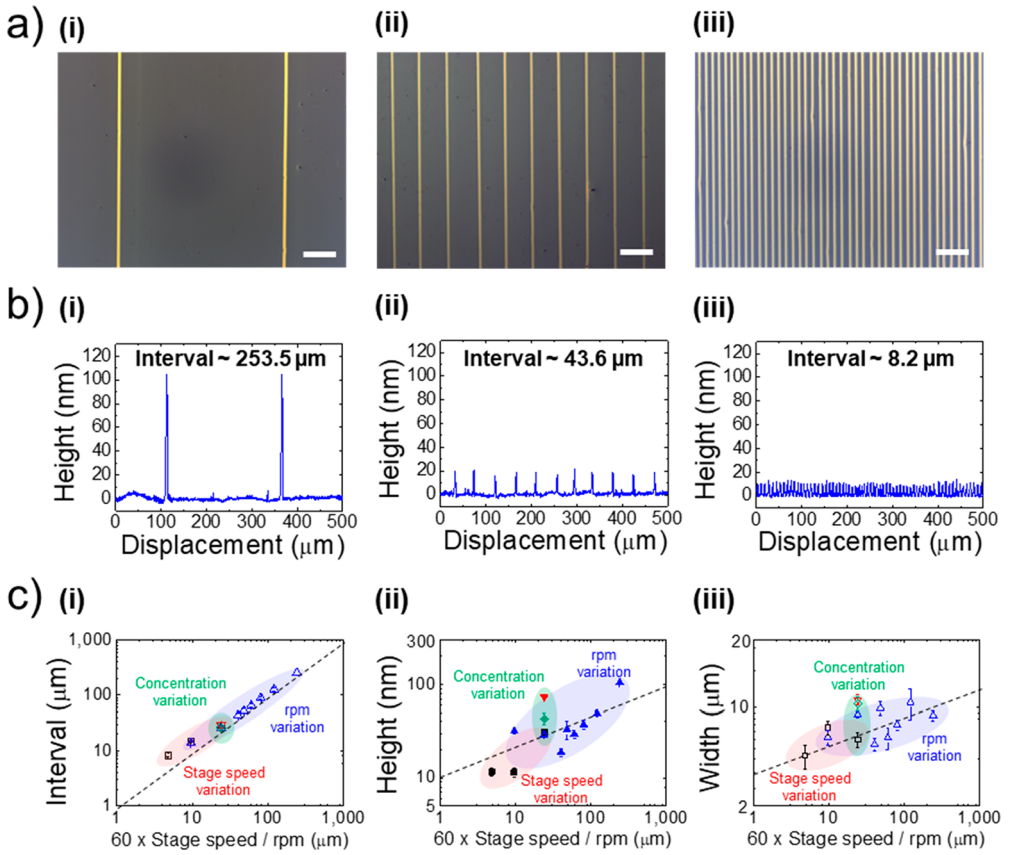

Figure 4. Hierarchically printed periodic P3HT line patterns. (a) Optical micrographs of P3HT lines at different printing conditions; scale bar, 50 μm: (i) low roller rotation speed (50 °C, 1 mg/mL P3HT in toluene; rotation speed, 250 rpm; stage speed, 1 mm/s); (ii) high roller rotation speed (50 °C, 1 mg/mL P3HT in toluene; rotation speed, 1500 rpm; stage speed, 1 mm/s); (iii) high roller rotation with low stage speed (50 °C, 1 mg/mL P3HT in toluene; rotation speed, 1250 rpm; stage speed, 0.1 mm/s). (b) Height profile of P3HT line patterns corresponding to (a). (c) Phase diagram of printed P3HT line patterns varied with the ratio of stage speed to roller rotation rpm: (i) interval phase diagram of P3HT line patterns; (ii) width (unfilled) and (iii) height (filled) trends of P3HT line patterns (black filled squares, black open squares, 0.5 mg/mL; blue filled triangles, blue open triangles, 1.0 mg/mL; red inverted filled triangles, red inverted open triangles, 2.0 mg/mL; aqua solid tilted square, aqua open tilted square, 5.0 mg/mL).

roller at 1250 rpm with 1 mm/s stage speed and the substrate at 50 °C, uniform width and line spacing of periodic P3HT patterns are achieved with highly defined edges as shown in Figure 2a-iii and Supporting Information, Figure S4. Moreover, the reproducibility of line formation is confirmed by identical printing results collected in the first and the second attempts under same experimental conditions (Supporting Information, Figure S5). As shear rates are regulated by the rotational speed of the continuously rotating roller, varying the rotational speed of roller is analogous to steady-shear experiments, not small amplitude oscillatory shear. Although disruption of the assembled structures was reported when steady shear was applied at 100 s^{-1},[25] the maximum steady shear used in this study was 1500 rpm or 25 s^{-1}, well below the shear rate of 100 s^{-1}. When the substrate was heated to 55 °C, solvent evaporation occurred too fast, such that the P3HT molecules were immobilized and had insufficient time to assemble into crystalline line patterns (Supporting Information, Figure S3b).

A photograph of P3HT lines patterned by MOSA on glass is shown in Figure 2b-i. After the continuous printing of P3HT, the centimeter scale sample presents a typical violet hue. With a tilted view (Figure 2b-ii), a bright-golden structural color was observed from reflecting color of nanometer-thick self-assembled structures.[34] The printed P3HT crystal patterns have large areas of uniform periodic line structures as shown in the green region (Figure 2c). The edge of the meniscus has curvilinear contact lines due to the free surface of the P3HT solution between the roller and substrate, resulting in parabolic flow patterns as the roller proceeds (red regions). In the case of roller rotation at zero rpm, the P3HT lines are formed perpendicular to the roller axis at its center, while the line is tilted at the inside and outside edges (Supporting Information, Figure S6).

The width, height, and line spacing were measured using a surface profilometer. For more precise measurement of width and height, atomic force microscopy (AFM) was utilized. The AFM surface profile and image are shown in Figure 2d-ii, iii, and Supporting Information, Figure S7, respectively. Printed P3HT crystals had nanometer-scale height (20−80 nm) and micrometer-scale width (1−3 μm), while the line spacing was submillimeter scale (10−240 μm). Note that in between P3HT line patterns, thin layers of P3HT (<1−10 nm) were found, similar to previous reports.[7,36] Despite the structural features spanning several length scales, these hierarchical P3HT crystals were printed continuously at a rate of 60 mm/min. The AFM images reveal very sharp and uniform edges for the few micrometer-scale width of P3HT crystals. Conductive AFM (C-AFM) reveals that the P3HT line patterns have higher conductivity and therefore higher crystallinity in comparison with flat surfaced P3HT (Supporting Information,

https://dx.doi.org/10.1021/acsnano.0c07268
ACS Nano XXXX, XXX, XXX−XXX

Figure S8). Higher conductivity levels at the P3HT line patterns imply effective electric charge transfer between thiophene groups. We normalized the current to thickness of P3HT by multiplying the current and P3HT thickness for calculation of conductivity using followed equation, $\sigma = IH/AV$ where I is current, H is thickness of P3HT, A is contact area of AFM tip, and V is applied voltage. The normalized conductivity as well as the electric current are drastically reduced at the boundary between the P3HT line and flat surfaced P3HT (Supporting Information, Figure S8c,d). As shear stress is the largest during the process of evaporative self-assembly, P3HT lines are expected to have the largest shear-induced crystallization and higher electrical current signal; this is verified by C-AFM (Supporting Information, Figure S8).

The influence of rotational shear on the crystallinity of P3HT line patterns was investigated by optical microscopy and grazing-incidence wide-angle X-ray scattering (GIWAXS) as shown in Figure 3. As a control group, P3HT was printed while the roller remained stationary. As visualized by optical microscopy, periodic patterns were not observed on the glass substrate in the case of 0 rpm for roller rotation (Figure 3a). At 1500 rpm of roller rotation, however, highly ordered periodic P3HT line patterns were printed on the glass substrate with uniform width and intervals (Figure 3b). To further elucidate the shear effect of the roller, GIWAXS experiments were carried out at different roller rotation rates (0, 250, 1000, and 1500 rpm) with two beam directions; parallel and perpendicular with respect to P3HT line patterns (Figure S9 and S10). When the X-ray beam was irradiated perpendicular to the long axis of the P3HT line patterns (Figure 3c-i), the intensity of the (100) peak increased for an out-of-plane scattering profile as the roller rotation rate increased, implying that the high shear accelerates the formation of P3HT crystals. Furthermore, there were no discernible peaks for the in-plane direction from the 2D scattering images (Figure 3c-iii,iv) even at high rotation rates. In the case of parallel X-ray irradiation (Figure 3d), there was only out-of-plane direction scattering in the 2D scattering image (Figure 3d-iv). For the out-of-plane scattering profile, as the rpm of roller increased, the intensity of the (100) peak of P3HT crystal also increased. As evident from the optical microscope and GIWAXS scattering, the imperfect crystal defects of P3HT are rapidly removed by the shear force of the roller rotation in both parallel and perpendicular directions in micro line patterns.

The capability of MOSA in engineering the width, height, and interval of P3HT crystal lines was investigated by examining various experimental parameters including rotation rate of roller, stage speed, and P3HT concentration. The dominant parameters that affect the spatial properties of the lines were the rotation rate of roller and the stage speed. Line spacing could be controlled in the range from a few micrometers to the submillimeter scale by varying rotation rate of roller in conjunction with the stage speed (Figure 4a,b, and Supporting Information, Figures S11–S15). As shown in Figure 4a-i,b-i, the low rotation rate and fast stage motion (250 rpm and 1 mm/s) induced low frequency of stick–slip motion along with a broad line spacing of 0.25 mm. While the stage moved 1 mm for 1 s, the roller rotated 4.2 times, resulting in an interval of approximately 0.25 mm. The 6-fold increase in rotation rate reduced the line spacing by a factor of 6 as evident from Figure 4a-ii,b-ii. As the roller rotation rate increased for the same volume of P3HT solution at a steady printing speed, the regulation of millimeter scale interval is achieved for the P3HT crystal lines with micrometer scale width and nanometer scale height (Supporting Information, Figure S12). In addition to the roller rotation rate, line spacing could also be controlled by varying the stage speed. At low stage speed, the displacement of the substrate changed the position of the line while the time-scale for pinning and depinning of contact line was identical (Supporting Information, Figure S14, and S15). By combining high rotation rate and slow stage speed, a line spacing of 8 μm is achieved (Figure 4a-iii,b-iii). The width and height of the line were not significantly altered with these variations in stage speed unlike the roller rotation rate because the frequency of contact line pinning and depinning is determined by roller rotation not by stage speed. The concentration of P3HT does not affect the frequency of roller motion but does impact line width and height (Supporting Information, Figure S16 and S17). The concentration of P3HT up to 2.0 mg/mL, the cross-section area of the line patterns is positively correlated to concentration. However, an excessively high concentration of P3HT (5.0 mg/mL) may obstruct the formation of the sharp crystal lines due to the increase in viscosity of the P3HT solution as the solvent evaporates (Supporting Information, Figure S17).[37] Increased viscosity induces P3HT coating of the substrate as well as a relatively blunt P3HT crystal line that decreases the height of line (Supporting Information, Figure S17a-iv,b-iv). The parameter study summarized in Figure 4c demonstrates the wide range of programmability for the interval, width, and height of solution processed organic crystals.

CONCLUSIONS

In this study, we have successfully demonstrated continuous printing of a semiconducting polymer, P3HT by a MOSA technique. This printing technique removes the dwell-time for contact-line formation typically required in convective deposition of P3HT, resulting in approximately 100 times faster printing at 60 mm/min printing speed. In addition to the fast printing rate, a wide range of engineering capability for hierarchical assembly was achieved including nanometer scale thickness (20–80 nm), micrometer scale width (1–3 μm) and micrometer to submillimeter interval (10–240 μm) with highly defined edge features. Importantly, each dimensional parameter was independently regulated by varying printing conditions. The shear-induced crystallization by the MOSA technique was shown to effectively remove imperfect crystal defects as evident from the GIWAXS experiments. The principles of MOSA elucidated by this work can be used to enable continuous self-assembly of functional polymers over arbitrary lengths of substrate by, for example, automating the dispensation of the polymer solution. Therefore, our work provides an efficient strategy toward high-throughput continuous printing of semiconducting polymers, encouraging future work on evaluating the material performance in devices, as well as application of the technique to other solution-based materials.

METHODS

Preparation of P3HT Solution. Poly(3-hexylthiophene) (P3HT) (Rieke Metals, Inc., EMI-001EE, M_w = 69 kDa, >96% regioregularity) was dissolved in toluene (Sigma-Aldrich) at 90 °C and stirred with a magnetic stir bar for 1 h. The concentration of P3HT solution was varied from 0.5 to 5 mg/mL.

https://dx.doi.org/10.1021/acsnano.0c07268
ACS Nano XXXX, XXX, XXX–XXX

MOSA Apparatus and Construction of P3HT Lines. The custom-made apparatus used to perform MOSA consists of a horizontally movable temperature-controlled sample stage and a roller (diameter = 2 mm, length = 35 mm) suspended above the sample stage by an H-frame. The temperature of the sample stage is regulated by thermoelectric chips (Custom Thermoelectric 12711-5L31-03CK) and a thermocouple (McMaster Carr 3648K24) in closed loop with a PID controller (Omega CNi32). The horizontal motion of the sample stage is driven by a precision linear actuator (Velmex X-Slide XN-10). The rotation of the roller is driven by a step motor (All Motion Products HT08-020D), where the shaft of the motor is connected to the roller by a flexible Tygon tube. The roller is supported by a bearing assembly on only one end, and the runout in the bearing assembly causes a periodic vertical motion with each rotation, measured to be 71 μm. The glass slide is attached to the stage equipped with a thermal heater, which is set to control the solvent evaporation rate. The stage speed, roller rotation speed, and temperature were controlled from a LabVIEW interface. In each experiment, the gap between the roller and sample stage was adjusted to 0.01 in. using a vertical stage micrometer connected to the roller. P3HT solution (20 μL) was dispensed at the gap by a hand pipet, after which the stage and roller motion was initiated immediately. The stage speed and roller rpm were varied from 0.1−5 mm/s and from 0−1500 rpm, respectively. The stage and roller motion were stopped when the P3HT solution dried out or when the end of the substrate was reached. As an option, the P3HT solution can be continuously dispensed by an automated pipet for continuous MOSA. For measurement of the current in the P3HT line, the MOSA process was implemented on an ITO glass under the condition: 50 °C stage, 1 mg/mL in toluene, stage speed 1.0 mm/s, and roller rotation 1250 rpm.

Grazing-Incidence Wide-Angle X-ray Scattering (GIWAXS). The P3HT line patterns were fabricated under these conditions: 50 °C stage, 1 mg/mL P3HT in toluene; stage speed, 1.0 mm/s; roller rotation 250 rpm, 1000 rpm, and 1500 rpm. GIWAXS experiments were performed at room temperature on beamline 3C at the Pohang Accelerator Laboratory (PAL) to investigate the crystallinity of P3HT line pattern with respect to roller blade rotation rpm. The operating wavelength was 0.15 nm, and a sample-to-detector distance was 0.2 m.

Characterization. The self-assembled micropatterns were photographed using an optical microscope (OM; ZEISS Axio Imager Z.1m upright microscope, AxioCam MRc5 CCD camera) in the reflection mode and scanning electron microscope (SEM; S-4300SE, Hitachi). The surface profile of P3HT line pattern was characterized by a profilometer (D-300, KLA-Tencor) and an atomic force microscope (AFM; Nanoscope Multimode IVa, Bruker). The current was measured by a current-sensing atomic force microscopy (CS-AFM; Agilent Technologies, Inc.) at an applied voltage (V) of 0.1 V (DC field) through a conductive Pt-coated ultrasharp silicon AFM tip (tip radius ~30 nm). The current flows in a downward direction from where the AFM tip comes in contact with the sample.

ASSOCIATED CONTENT

Supporting Information

The Supporting Information is available free of charge at https://pubs.acs.org/doi/10.1021/acsnano.0c07268.

Illustration and digital image of MOSA setup; optical micrographs; SEM analysis; AFM analysis; calculation of conductivity; GIWAXS analysis; height profile of P3HT patterns with different conditions (PDF)

AUTHOR INFORMATION

Corresponding Authors

Jeong Jae Wie − *Department of Polymer Science and Engineering and Program in Environmental and Polymer Engineering, Inha University, Incheon 22212, Republic of Korea;* orcid.org/0000-0001-7381-947X; Phone: 82-32-860-7484; Email: wie@inha.ac.kr

A. John Hart − *Department of Mechanical Engineering and Laboratory for Manufacturing and Productivity, Massachusetts Institute of Technology, Cambridge, Massachusetts 02139, United States;* orcid.org/0000-0002-7372-3512; Email: ajhart@mit.edu

Authors

Jisoo Jeon − *Department of Polymer Science and Engineering and Program in Environmental and Polymer Engineering, Inha University, Incheon 22212, Republic of Korea;* orcid.org/0000-0002-0969-0293

Alvin T. L. Tan − *Department of Mechanical Engineering and Laboratory for Manufacturing and Productivity, Massachusetts Institute of Technology, Cambridge, Massachusetts 02139, United States*

Jaeyong Lee − *Department of Chemical Engineering, Pohang University of Science and Technology, Pohang, Kyungbuk 37673, Republic of Korea*

Jeong Eun Park − *Department of Polymer Science and Engineering and Program in Environmental and Polymer Engineering, Inha University, Incheon 22212, Republic of Korea*

Sukyoung Won − *Department of Polymer Science and Engineering and Program in Environmental and Polymer Engineering, Inha University, Incheon 22212, Republic of Korea*

Sanha Kim − *Department of Mechanical Engineering and Laboratory for Manufacturing and Productivity, Massachusetts Institute of Technology, Cambridge, Massachusetts 02139, United States;* orcid.org/0000-0002-3548-6173

Mostafa Bedewy − *Department of Industrial Engineering, University of Pittsburgh, Pittsburgh, Pennsylvania 15261, United States;* orcid.org/0000-0003-4182-7533

Jamison Go − *Department of Mechanical Engineering and Laboratory for Manufacturing and Productivity, Massachusetts Institute of Technology, Cambridge, Massachusetts 02139, United States*

Jin Kon Kim − *Department of Chemical Engineering, Pohang University of Science and Technology, Pohang, Kyungbuk 37673, Republic of Korea;* orcid.org/0000-0002-3872-2004

Complete contact information is available at: https://pubs.acs.org/10.1021/acsnano.0c07268

Author Contributions

#J.J. and A.T.L.T. these authors contributed equally

Notes

The authors declare no competing financial interest.

ACKNOWLEDGMENTS

This work was supported by the Inha University research grant (59398-1) to J.J.W., the NSF-CAREER Award (CMMI-134663) and NSF-GOALI (1463181) to A.J.H, and the National Creative Research Initiative Program supported by the National Research Foundation of Korea (2013R1A3A2042196) to J.K.K. A.T.L.T. was supported by a postgraduate fellowship from DSO National Laboratories, Singapore). J.J.W. thanks Prof. Jin-Kyun Lee for facilitating the use of profiler for width and height characterization.

https://dx.doi.org/10.1021/acsnano.0c07268
ACS Nano XXXX, XXX, XXX−XXX

REFERENCES

(1) Gu, X.; Shaw, L.; Gu, K.; Toney, M. F.; Bao, Z. The Meniscus-Guided Deposition of Semiconducting Polymers. *Nat. Commun.* **2018**, *9*, 534.

(2) Yuan, Y.; Giri, G.; Ayzner, A. L.; Zoombelt, A. P.; Mannsfeld, S. C. B.; Chen, J.; Nordlund, D.; Toney, M. F.; Huang, J.; Bao, Z. Ultra-High Mobility Transparent Organic Thin Film Transistors Grown by an Off-Centre Spin-Coating Method. *Nat. Commun.* **2014**, *5*, 3005.

(3) Ko, J.; Kim, Y.; Kang, J. S.; Berger, R.; Yoon, H.; Char, K. Enhanced Vertical Charge Transport of Homo- and Blended Semiconducting Polymers by Nanoconfinement. *Adv. Mater.* **2020**, *32*, 1908087.

(4) Jung, E. H.; Jeon, N. J.; Park, E. Y.; Moon, C. S.; Shin, T. J.; Yang, T. Y.; Noh, J. H.; Seo, J. Efficient, Stable and Scalable Perovskite Solar Cells Using Poly(3-Hexylthiophene). *Nature* **2019**, *567*, 511−515.

(5) Kim, B. G.; Jeong, E. J.; Chung, J. W.; Seo, S.; Koo, B.; Kim, J. A Molecular Design Principle of Lyotropic Liquid-Crystalline Conjugated Polymers with Directed Alignment Capability for Plastic Electronics. *Nat. Mater.* **2013**, *12*, 659−664.

(6) Shin, J. I.; Cho, S. J.; Jeon, J.; Lee, K. H.; Wie, J. J. Three-Dimensional Micropatterning of Semiconducting Polymers: *Via* Capillary Force-Assisted Evaporative Self-Assembly. *Soft Matter* **2019**, *15*, 3854−3863.

(7) Park, W. I.; Kim, D. H.; Jung, J.; Hong, S. W.; Lin, Z.; Byun, M. Spatially Ordered Poly(3-Hexylthiophene) Fibril Nanostructures *via* Controlled Evaporative Self-Assembly. *Adv. Mater. Technol.* **2019**, *4*, 1800554.

(8) Han, W.; He, M.; Byun, M.; Li, B.; Lin, Z. Large-Scale Hierarchically Structured Conjugated Polymer Assemblies with Enhanced Electrical Conductivity. *Angew. Chem., Int. Ed.* **2013**, *52*, 2564−2568.

(9) Cho, H. R.; Park, W. I.; Song, Y. S.; Jung, J.; Choe, A.; Ko, H.; Byun, M. Spontaneous Capillary Breakup of Suspended Gradient Polymer Stripes into Spatially Ordered Dot Arrays. *Appl. Surf. Sci.* **2019**, *475*, 1003−1009.

(10) Li, X.; Li, B.; He, M.; Wang, W.; Wang, T.; Wang, A.; Yu, J.; Wang, Z.; Hong, S. W.; Byun, M.; Lin, S.; Yu, H.; Lin, Z. Convenient and Robust Route to Photoswitchable Hierarchical Liquid Crystal Polymer Stripes *via* Flow-Enabled Self-Assembly. *ACS Appl. Mater. Interfaces* **2018**, *10*, 4961−4970.

(11) Li, B.; Han, W.; Byun, M.; Zhu, L.; Zou, Q.; Lin, Z. Macroscopic Highly Aligned DNA Nanowires Created by Controlled Evaporative Self-Assembly. *ACS Nano* **2013**, *7*, 4326−4333.

(12) Li, B.; Han, W.; Jiang, B.; Lin, Z. Crafting Threads of Diblock Copolymer Micelles *via* Flow-Enabled Self-Assembly. *ACS Nano* **2014**, *8*, 2936−2942.

(13) Han, M. J.; Kim, J.; Kim, B.; Park, S. M.; Ahn, H.; Shin, T. J.; Kim, B.; Kim, H.; Yoon, D. K. Orientation Control of Semiconducting Polymers Using Microchannel Molds. *ACS Nano* **2020**, *14* (10), 12951−12961.

(14) Lawrence, J.; Pham, J. T.; Lee, D. Y.; Liu, Y.; Crosby, A. J.; Emrick, T. Highly Conductive Ribbons Prepared by Stick-Slip Assembly of Organosoluble Gold Nanoparticles. *ACS Nano* **2014**, *8*, 1173−1179.

(15) Liu, Y.; Lee, D. Y.; Monteux, C.; Crosby, A. J. Hyperbranched Polymer Structures *via* Flexible Blade Flow Coating. *J. Polym. Sci., Part B: Polym. Phys.* **2016**, *54*, 32−37.

(16) Byun, M.; Han, W.; Qiu, F.; Bowden, N. B.; Lin, Z. Hierarchically Ordered Structures Enabled by Controlled Evaporative Self-Assembly. *Small* **2010**, *6*, 2250−2255.

(17) Hong, S. W.; Byun, M.; Lin, Z. Robust Self-Assembly of Highly Ordered Complex Structures by Controlled Evaporation of Confined Microfluids. *Angew. Chem., Int. Ed.* **2009**, *48*, 512−516.

(18) Byun, M.; Bowden, N. B.; Lin, Z. Hierarchically Organized Structures Engineered from Controlled Evaporative Self-Assembly. *Nano Lett.* **2010**, *10*, 3111−3117.

(19) Byun, M.; Han, W.; Li, B.; Xin, X.; Lin, Z. An Unconventional Route to Hierarchically Ordered Block Copolymers on a Gradient Patterned Surface through Controlled Evaporative Self-Assembly. *Angew. Chem., Int. Ed.* **2013**, *52*, 1122−1127.

(20) Byun, M.; Laskowski, R. L.; He, M.; Qiu, F.; Jeffries-El, M.; Lin, Z. Controlled Evaporative Self-Assembly of Hierarchically Structured Regioregular Conjugated Polymers. *Soft Matter* **2009**, *5*, 1583−1586.

(21) Park, W. K.; Kim, T.; Kim, H.; Kim, Y.; Tung, T. T.; Lin, Z.; Jang, A. R.; Shin, H. S.; Han, J. H.; Yoon, D. H.; Yang, W. S. Large-Scale Patterning by the Roll-Based Evaporation-Induced Self-Assembly. *J. Mater. Chem.* **2012**, *22*, 22844−22847.

(22) Choudhary, S.; Crosby, A. J. Controlled Evaporative Self-Assembly of Polymer Nanoribbons Using Oscillating Capillary Bridges. *J. Polym. Sci., Part B: Polym. Phys.* **2018**, *56*, 1545−1551.

(23) Farcau, C.; Moreira, H.; Viallet, B.; Grisolia, J.; Ressier, L. Tunable Conductive Nanoparticle Wire Arrays Fabricated by Convective Self-Assembly on Nonpatterned Substrates. *ACS Nano* **2010**, *4*, 7275−7282.

(24) Lim, J. A.; Liu, F.; Ferdous, S.; Muthukumar, M.; Briseno, A. L. Polymer Semiconductor Crystals. *Mater. Today* **2010**, *13*, 14−24.

(25) Wie, J. J.; Nguyen, N. A.; Cwalina, C. D.; Liu, J.; Martin, D. C.; Mackay, M. E. Shear-Induced Solution Crystallization of Poly(3-Hexylthiophene) (P3HT). *Macromolecules* **2014**, *47*, 3343−3349.

(26) Iovu, M. C.; Jeffries-El, M.; Sheina, E. E.; Cooper, J. R.; McCullough, R. D. Regioregular Poly(3-Alkylthiophene) Conducting Block Copolymers. *Polymer* **2005**, *46*, 8582−8586.

(27) Babel, A.; Zhu, Y.; Cheng, K. F.; Chen, W. C.; Jenekhe, S. A. High Electron Mobility and Ambipolar Charge Transport in Binary Blends of Donor and Acceptor Conjugated Polymers. *Adv. Funct. Mater.* **2007**, *17*, 2542−2549.

(28) Coakley, K. M.; Liu, Y.; McGehee, M. D.; Frindell, K. L.; Stucky, G. D. Infiltrating Semiconducting Polymers into Self-Assembled Mesoporous Titania Films for Photovoltaic Applications. *Adv. Funct. Mater.* **2003**, *13*, 301−306.

(29) Jeffries-El, M.; Sauvé, G.; McCullough, R. D. *In-Situ* End-Group Functionalization of Regioregular Poly(3-Alkylthiophene) Using the Grignard Metathesis Polymerization Method. *Adv. Mater.* **2004**, *16*, 1017−1019.

(30) Jeffries-El, M.; Sauvé, G.; McCullough, R. D. Facile Synthesis of End-Functionalized Regioregular Poly(3-Alkylthiophene)s *via* Modified Grignard Metathesis Reaction. *Macromolecules* **2005**, *38*, 10346−10352.

(31) Sheina, E. E.; Liu, J.; Iovu, M. C.; Laird, D. W.; McCullough, R. D. Chain Growth Mechanism for Regioregular Nickel-Initiated Cross-Coupling Polymerizations. *Macromolecules* **2004**, *37*, 3526−3528.

(32) Yang, H.; Shin, T. J.; Yang, L.; Cho, K.; Ryu, C. Y.; Bao, Z. Effect of Mesoscale Crystalline Structure on the Field-Effect Mobility of Regioregular Poly(3-Hexyl Thiophene) in Thin-Film Transistors. *Adv. Funct. Mater.* **2005**, *15*, 671−676.

(33) Roesing, M.; Howell, J.; Boucher, D. Solubility Characteristics of Poly(3-Hexylthiophene). *J. Polym. Sci., Part B: Polym. Phys.* **2017**, *55*, 1075−1087.

(34) Inganäs, O.; Salaneck, W. R.; Österholm, J. -E.; Laakso, J. Thermochromic and Solvatochromic Effects in Poly(3-Hexylthiophene). *Synth. Met.* **1988**, *22*, 395−406.

(35) Hohmann, C.; Stephan, P. Microscale Temperature Measurement at an Evaporating Liquid Meniscus. *Exp. Therm. Fluid Sci.* **2002**, *26*, 157−162.

(36) Xiao, G.; Guo, Y.; Lin, Y.; Ma, X.; Su, Z.; Wang, Q. Controlled Evaporative Self-Assembly of Poly(3-Hexylthiophene) Monitored with Confocal Polarized Raman Spectroscopy. *Phys. Chem. Chem. Phys.* **2012**, *14*, 16286−16293.

(37) Sun, Y.; Xiao, G.; Lin, Y.; Su, Z.; Wang, Q. Self-Assembly of Large-Scale P3HT Patterns by Confined Evaporation in the Capillary Tube. *RSC Adv.* **2015**, *5*, 20491−20497.

https://dx.doi.org/10.1021/acsnano.0c07268
ACS Nano XXXX, XXX, XXX−XXX

Supporting Information

High-Speed Production of Crystalline Semiconducting Polymer Line Arrays by Meniscus Oscillation Self-Assembly

Jisoo Jeon,[1,2,#] Alvin T.L. Tan,[3,#] Jaeyong Lee,[4] Jeong Eun Park,[1,2] Sukyoung Won,[1,2] Sanha Kim,[3] Mostafa Bedewy,[5] Jamison Go,[3] Jin Kon Kim,[4] A. John Hart,[3,] Jeong Jae Wie,[1,2,*]*

[1]Inha University, Department of Polymer Science and Engineering, Incheon 22212, Republic of Korea

[2]Inha University, Program in Environmental and Polymer Engineering, Incheon 22212, Republic of Korea

[3]Massachusetts Institute of Technology, Department of Mechanical Engineering and Laboratory for Manufacturing and Productivity, Cambridge, MA 02139, USA

[4]Pohang University of Science and Technology, Department of Chemical Engineering, Pohang, Kyungbuk 37673, Republic of Korea

[5]University of Pittsburgh, Department of Industrial Engineering, Pittsburgh, PA 15261, USA

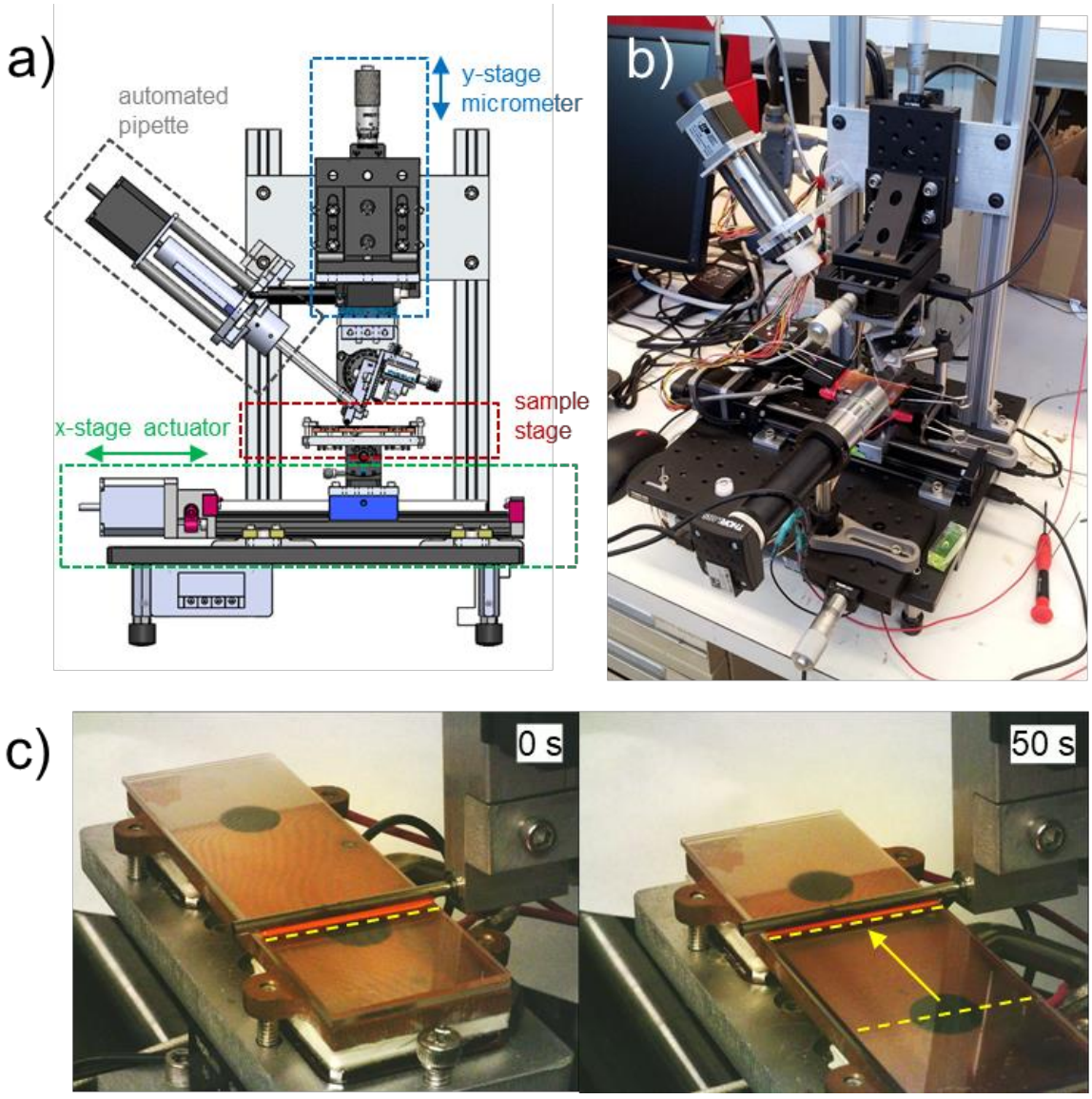

Figure S1. (a) Illustration and (b) photograph of the custom apparatus for meniscus oscillation self-assembly. (c) Time-scales of P3HT line formation by MOSA technique.

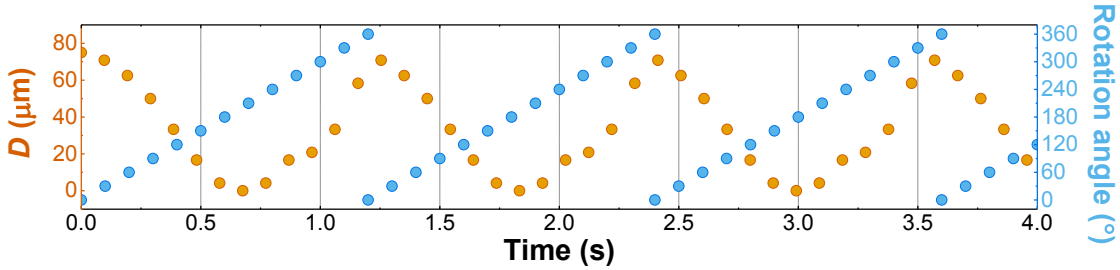

Figure S2. The time-resolved graph showing the apex position of the roller (D=0) relative to its maximum position, and rotation angle, rotation speed: 50 rpm.

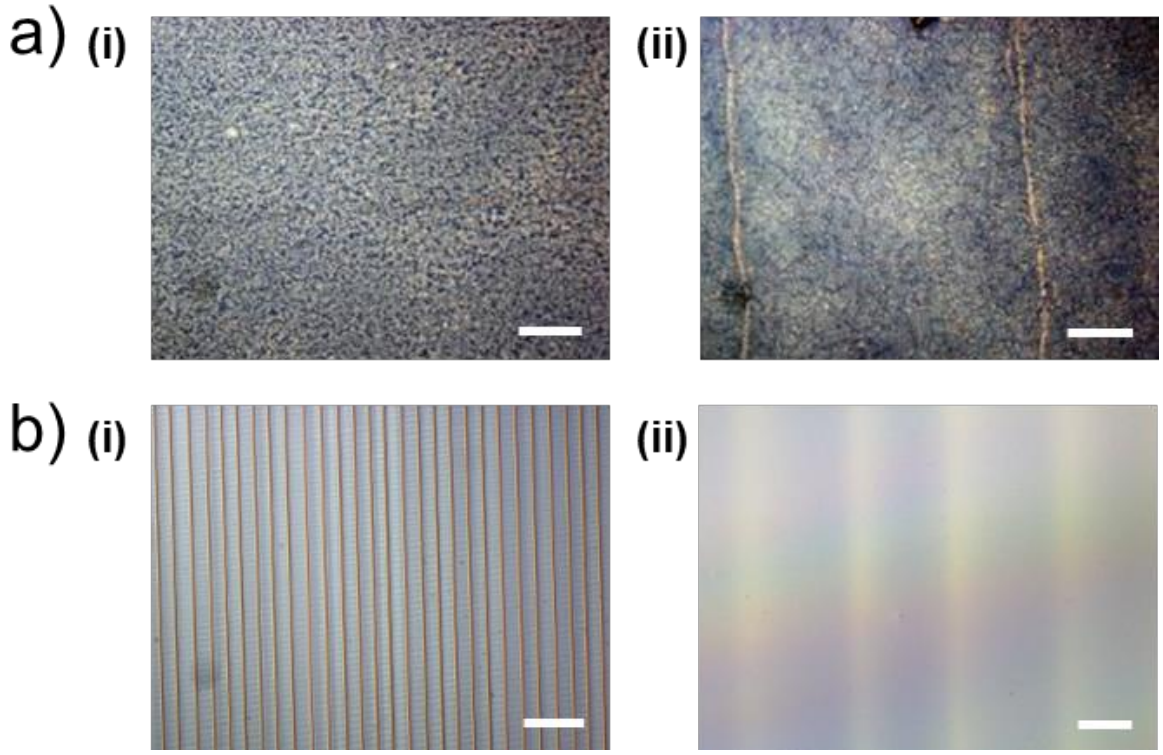

Figure S3. Optical micrographs of P3HT after MOSA process at different conditions. (a) P3HT roller blading at room temperature, (i) 0 rpm, (ii) 500 rpm (25 °C stage, 5 mg/mL P3HT in toluene, scale bars: 50 µm). (b) MOSA process at different temperature (i) 50 °C stage, scale bar: 50 um, (ii) 55 °C stage (5 mg/mL P3HT in toluene, rotation speed: 1250 rpm, stage speed: 1 (i) & 2 (ii) mm/s, scale bar: 200 µm).

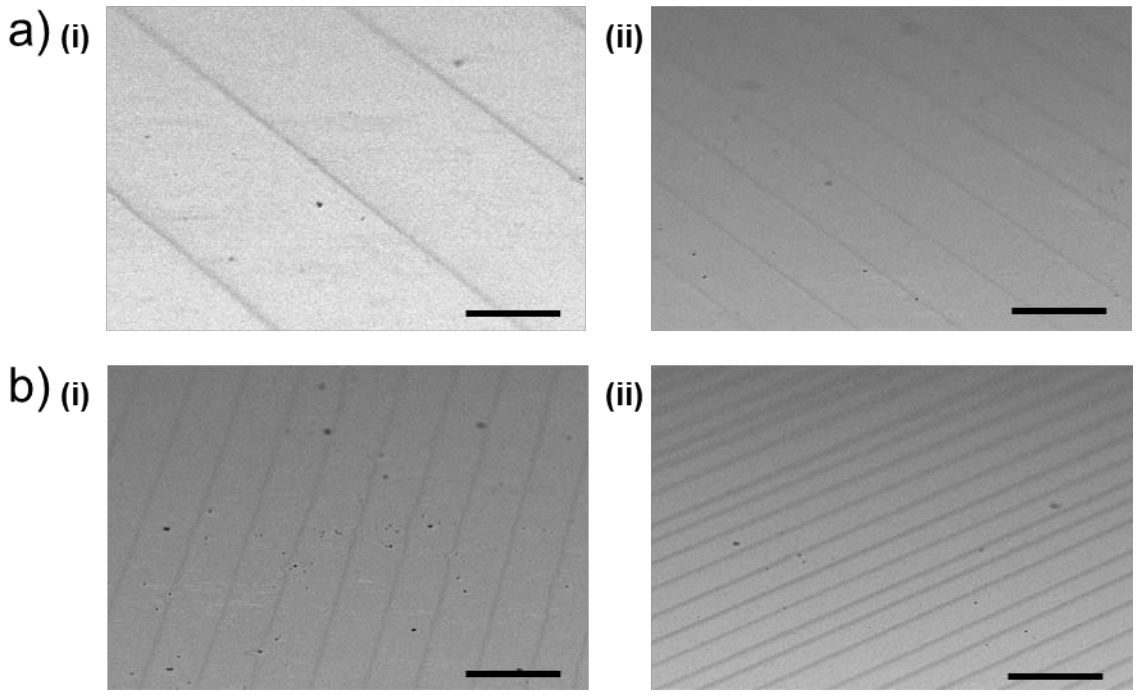

Figure S4. SEM micrographs of P3HT line pattern, scale bar: 50 µm. (a) Roller rpm variation, (i) 500 rpm, (ii) 1250 rpm (50 ºC stage, 1.0 mg/mL P3HT in toluene, stage speed: 1.0 mm/s). (b) Concentration variation, (i) 0.5 mg/mL, (ii) 2.0 mg/mL (50 ºC Stage, speed of roller rotation: 1250 rpm, stage speed: 0.5 mm/s).

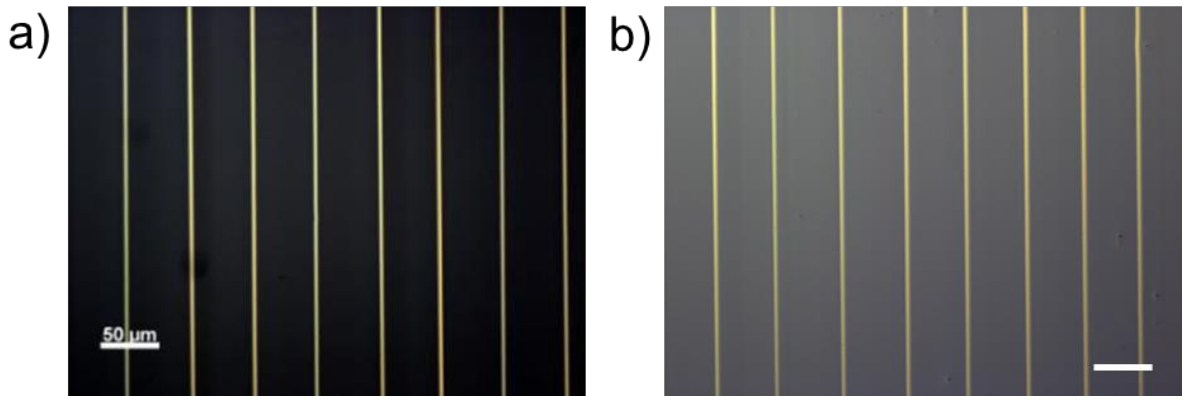

Figure S5. Reproducibility of MOSA process. (a) 1st attempt, (b) 2nd attempt, scale bar: 50 µm (1 mg/mL P3HT in toluene, 50 ºC stage, rotation speed of roller: 1250 rpm, stage speed: 1 mm/s).

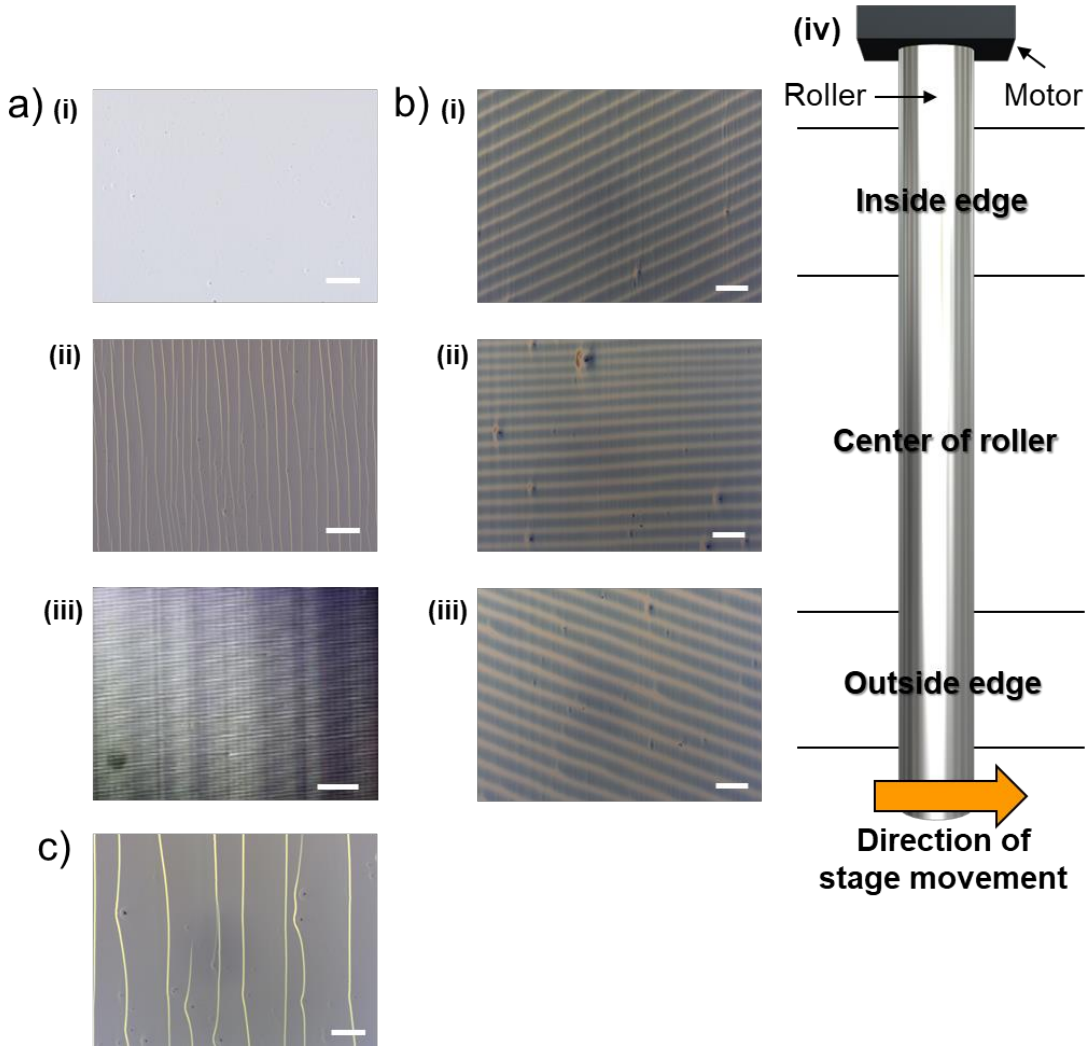

Figure S6. (a) MOSA process without rotation of roller at different stage speed and concentrations at 50 °C stage, (i) 1 mg/mL P3HT in toluene, stage speed: 1 mm/s, (ii) 1 mg/mL P3HT in toluene, stage speed: 0.5 mm/s, (iii) 5 mg/mL P3HT in toluene, stage speed: 1 mm/s (scale bars: 200 µm). (b) P3HT pattern without rotation of roller at different position in roller: (i) inside of roller; (ii) center of roller; (iii) outside of roller; (iv) schematic illustration of roller and direction of stage movement (5 mg/mL P3HT in toluene, stage speed: 0.5 mm/s, scale bar: 50 µm). (c) P3HT line pattern without roller rotation, (rotation speed: 0 rpm, 50 °C stage, 1 mg/mL P3HT in toluene, stage speed: 0.5 mm/s).

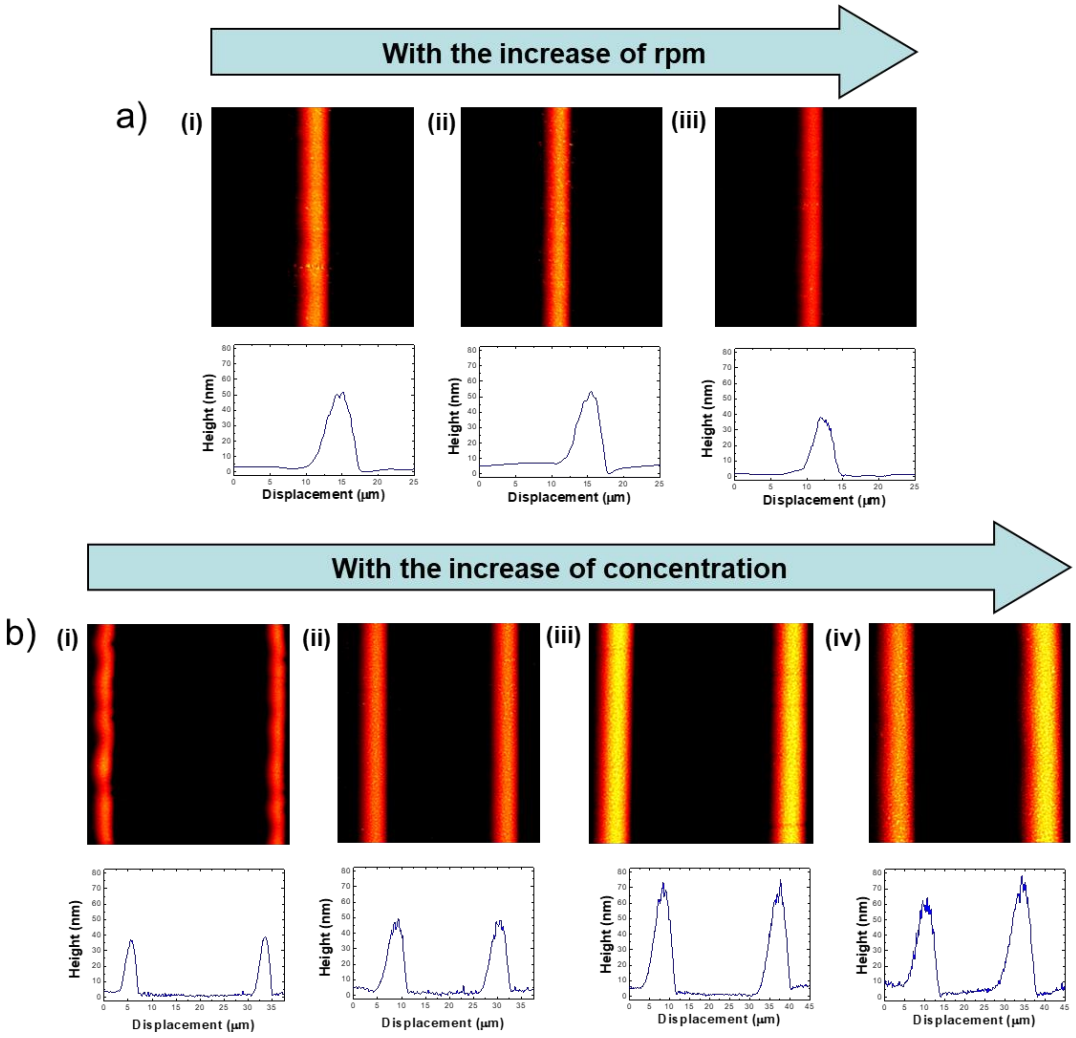

Figure S7. Atomic force microscope (AFM) of P3HT line at different conditions. (a) Roller rpm variations: (i) 500 rpm; (ii) 750 rpm; (iii) 1250 rpm (50 ºC stage, stage speed: 1.0 mm/s). (b) Variations of P3HT concentration: (i) 0.5 mg/mL; (ii) 1.0 mg/mL; (iii) 2.0 mg/mL; (iv) 5.0 mg/mL (50 ºC Stage, stage speed: 0.5 mm/s).

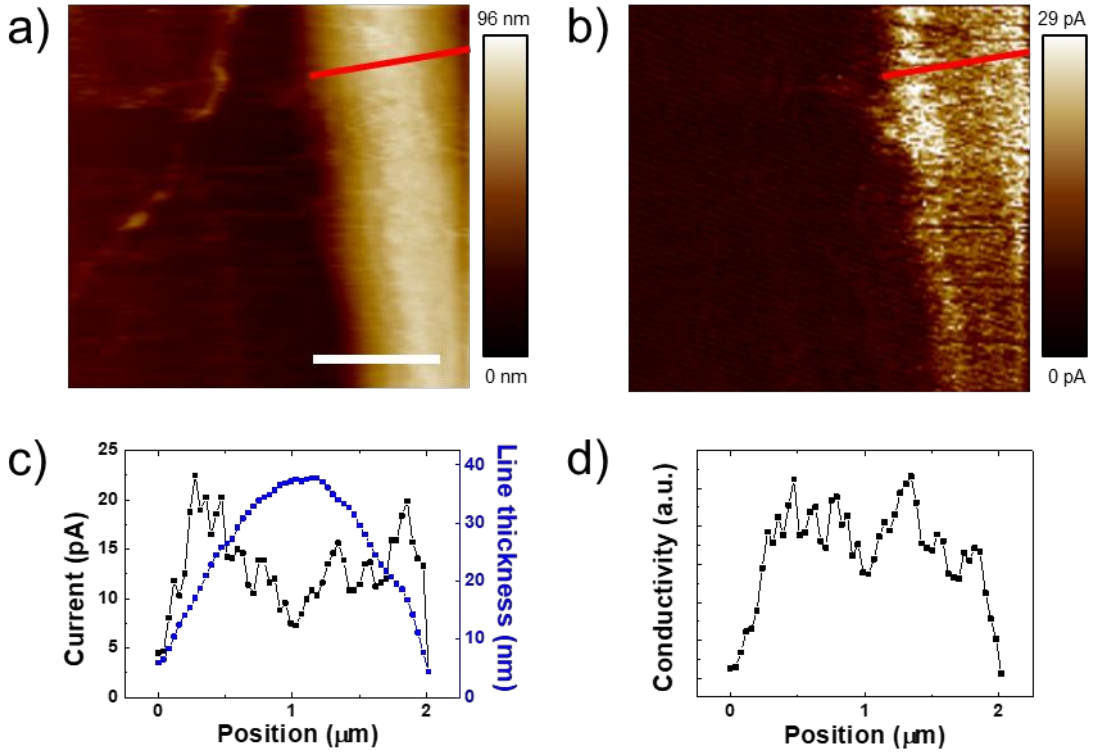

Figure S8. (a) Topology and (b) current measurements by conductive force microscope (C-AFM) for flat and crystallite line of P3HT on ITO substrate. (c) Current and line thickness, and (d) the conductivity (σ) profile across the P3HT line. The position in (c and d) corresponds to the position in the red line in (a) and (b).

Calculation of conductivity of P3HT line pattern

We calculated the conductivity (σ) from the measured conductance (C) using the information of line thickness (H) and AFM tip surface area (A) under same voltage (V).

$$C = \frac{I}{V}, \qquad C = \sigma\frac{A}{H}, \qquad \sigma = \frac{IH}{AV}$$

As the conductivity (σ) is related with the product of current (I) and line thickness (H), we picked one position to compare the current and line thickness profile (red line in Figure S8a or S8b). The current is measured in a downward direction from where the AFM tip contacts the sample. We traced the conductivity differences along the crystallite P3HT lines by multiplying the current and line thickness.

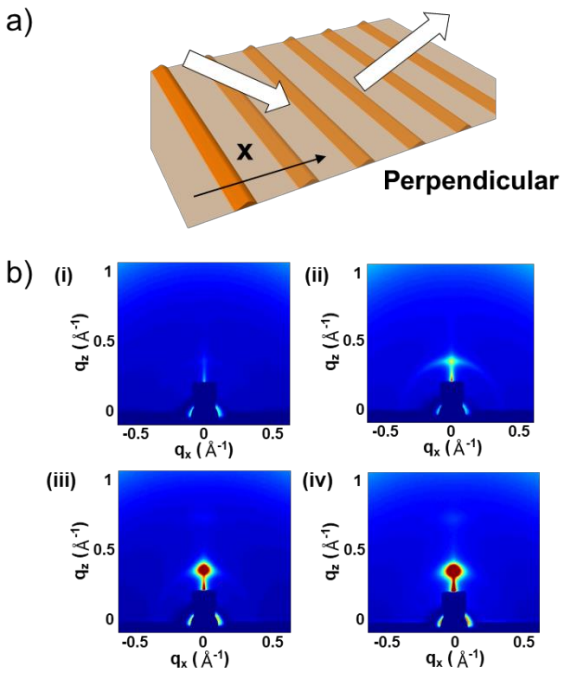

Figure S9. GIWAXS patterns of P3HT crystal on the slide glass (Beam direction ⊥ P3HT line). (a) Schematic illustration of beam irradiation. (b) GIWAXS patterns of P3HT crystal corresponding to roller speed, (i) 0 rpm, (ii) 250 rpm, (iii) 1000 rpm, (iv) 1500 rpm (50℃ stage, 1 mg/mL P3HT in toluene, stage speed: 1.0 mm/s).

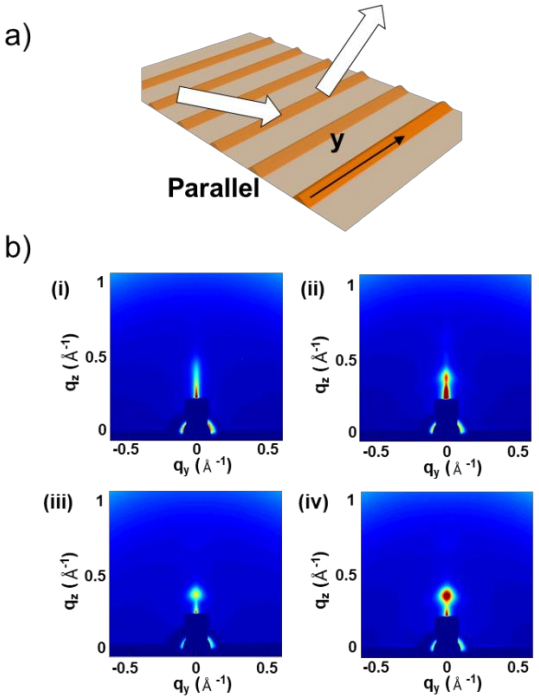

Figure S10. GIWAXS patterns of P3HT crystal on the slide glass (beam direction // P3HT line). (a) Schematic illustration of beam irradiation. (b) GIWAXS patterns of P3HT crystal corresponding to roller speed: (i) 0 rpm; (ii) 250 rpm; (iii) 1000 rpm; (iv) 1500 rpm (50 ℃ stage, 1 mg/mL P3HT in toluene, stage speed: 1.0 mm/s).

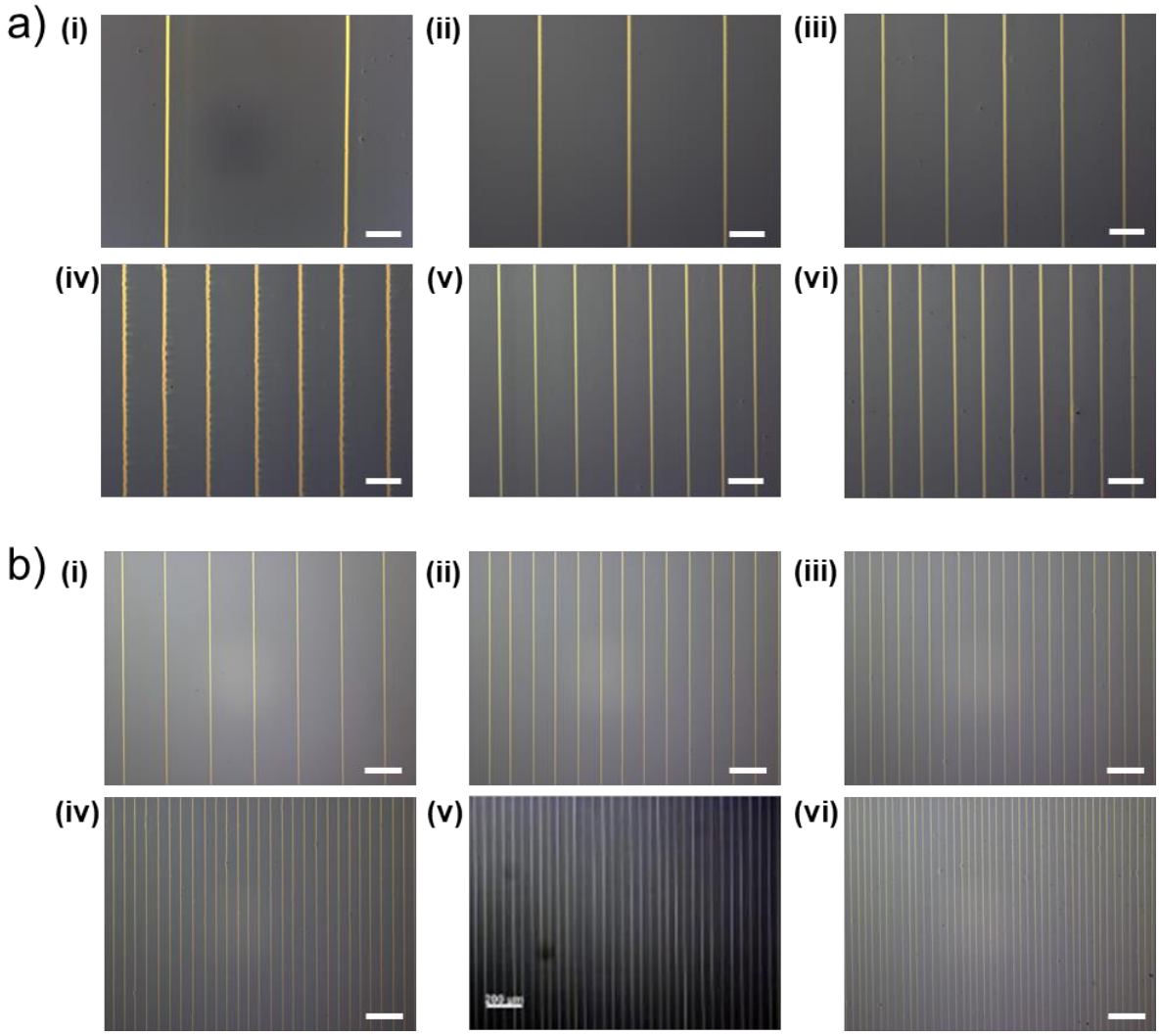

Figure S11. Optical micrographs of interval variation of P3HT line pattern at different roller rpm (250 rpm to 1500 rpm) high magnification optical micrographs (20x). (b) Low magnification optical micrographs (10x) (50 ºC Stage, 1 mg/mL P3HT in toluene, stage speed: 1 mm/s): (i) 250 rpm; (ii) 500 rpm; (iii) 750 rpm; (iv) 1000 rpm; (v) 1250 rpm; (vi) 1500 rpm.

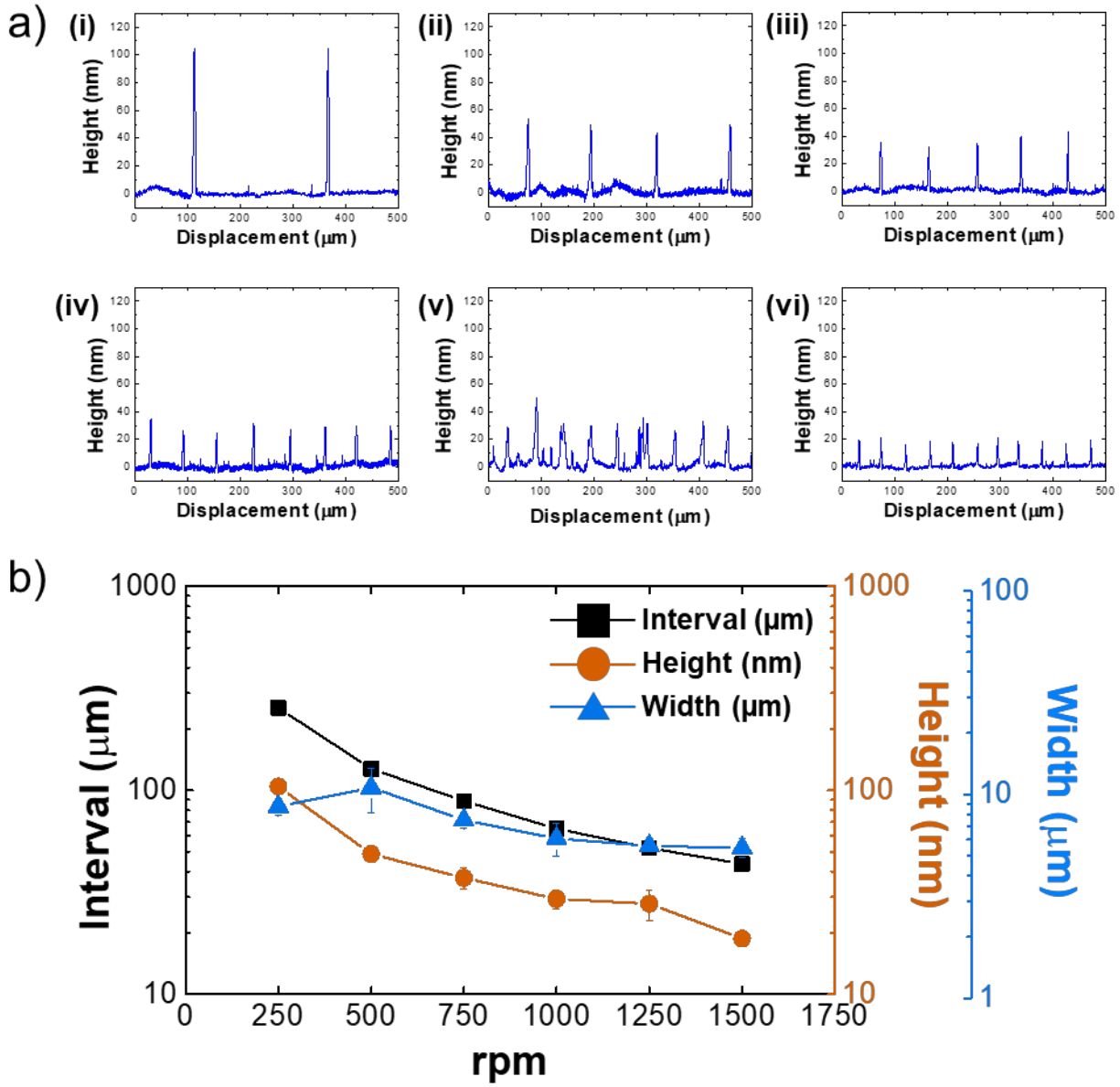

Figure S12. Height profile of P3HT line pattern with different roller rpm. (a) Roller rpm variations: (i) 250 rpm; (ii) 500 rpm; (iii) 750 rpm; (iv) 1000 rpm; (v) 1250 rpm; (vi) 1500 rpm (250 rpm to 1500 rpm) (50 ºC stage, 1 mg/mL P3HT in toluene, stage speed: 1.0 mm/s). (b) Summary of interval, height, and width of line pattern with different roller rpm.

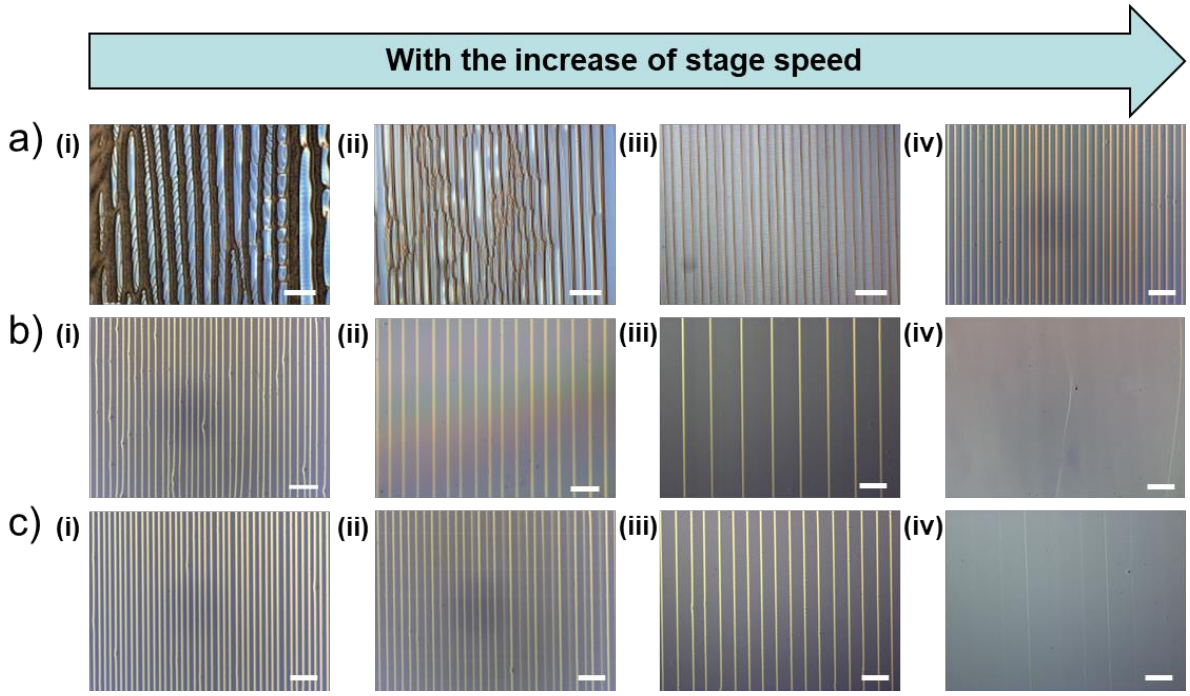

Figure S13. Optical micrographs of interval regulated P3HT line pattern by varying stage speed at different concentration. (a) MOSA process at 5.0 mg/mL P3HT in toluene; (i) 0.01 mm/s, (ii) 0.1 mm/s, (iii) 0.5 mm/s, and (iv) 1.0 mm/s, scale bar: 200 µm (b) P3HT roller blading at 1.0 mg/mL P3HT in toluene: (i) 0.2 mm/s; (ii) 0.5 mm/s; (iii) 1.0 mm/s; (iv) 2.0 mm/s, scale bar: 50 µm. (c) MOSA process at 0.5 mg/mL P3HT in toluene: (i) 0.1 mm/s; (ii) 0.2 mm/s; (iii) 0.5 mm/s; (iv) 1.0 mm/s, scale bar: 50 µm (50 ºC stage, rotation speed: 1250 rpm).

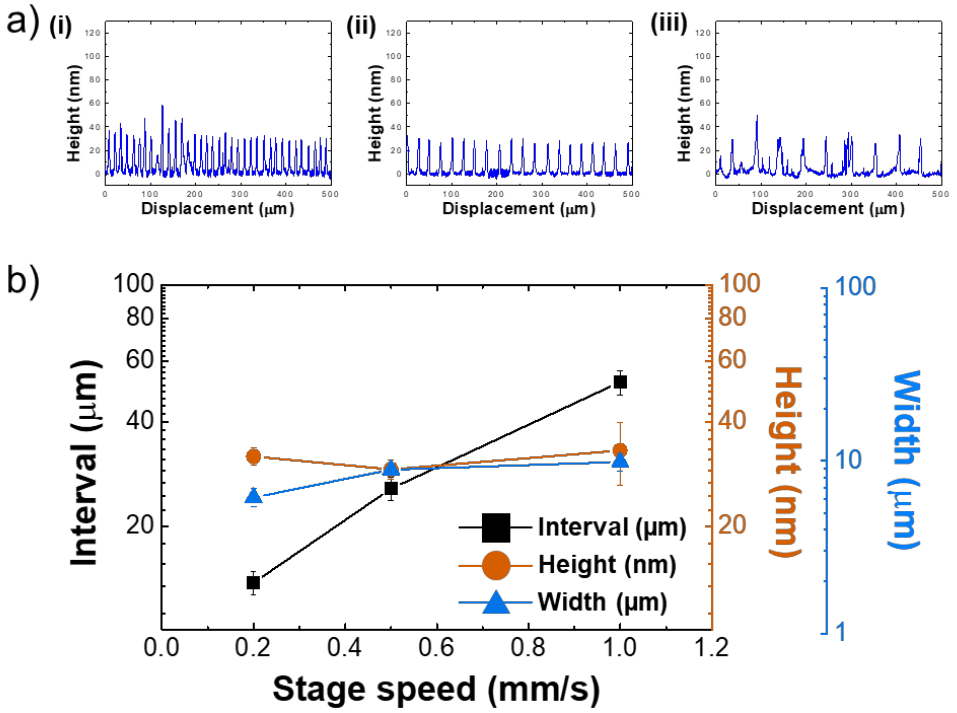

Figure S14. Height profile of P3HT line pattern with different stage speed. (a) Stage speed variations: (i) 0.2 mm/s; (ii) 0.5 mm/s; (iii) 1.0 mm/s (50 ºC stage, speed of roller rotation: 1250 rpm, 1 mg/mL P3HT in toluene). (b) Summary of interval, height, and width of line pattern with different stage speed.

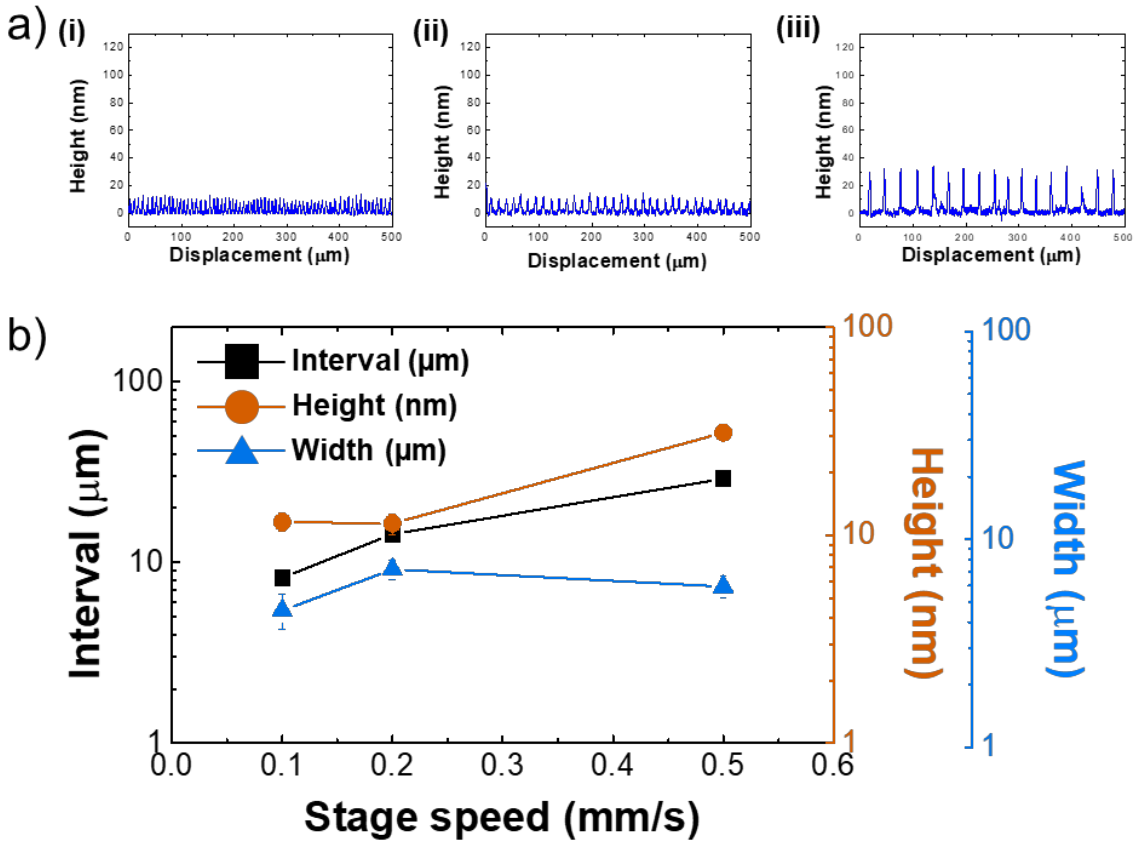

Figure S15. Height profile of P3HT line pattern with different stage speed. (a) Stage speed variations: (i) 0.1 mm/s; (ii) 0.2 mm/s; (iii) 0.5 mm/s (50 ºC stage, speed of roller rotation: 1250 rpm, 0.5 mg/mL P3HT in toluene). (b) Summary of interval, height, and width of line pattern with different stage speed.

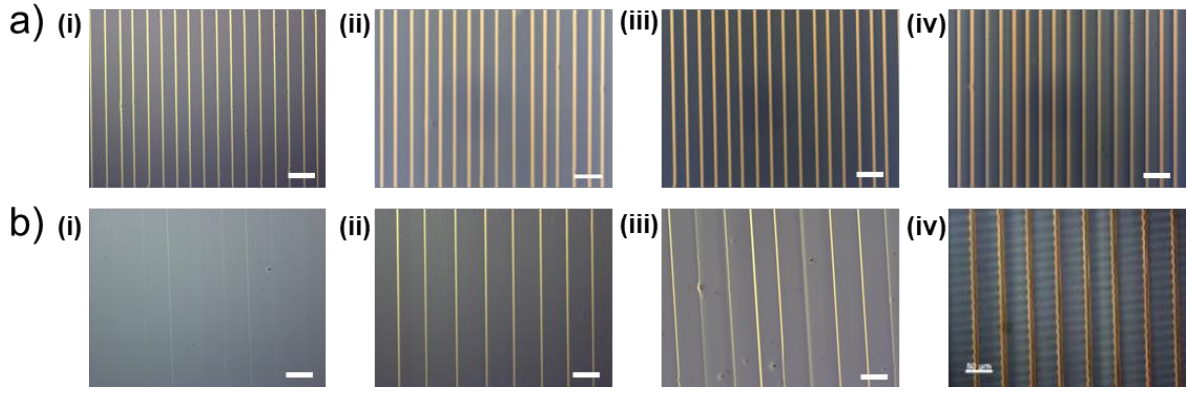

Figure S16. Optical micrographs of P3HT line pattern at different P3HT concentration. (a) 50 ºC stage, speed of roller rotation: 1250 rpm stage speed: 0.5 mm/s. (b) 50 ºC stage, speed of roller rotation: 1250 rpm, stage speed: 1.0 mm/s, Scale bar: 50 μm; (i) 0.5 mg/mL; (ii) 1.0 mg/mL; (iii) 2 mg/mL; (iv) 5 mg/mL.

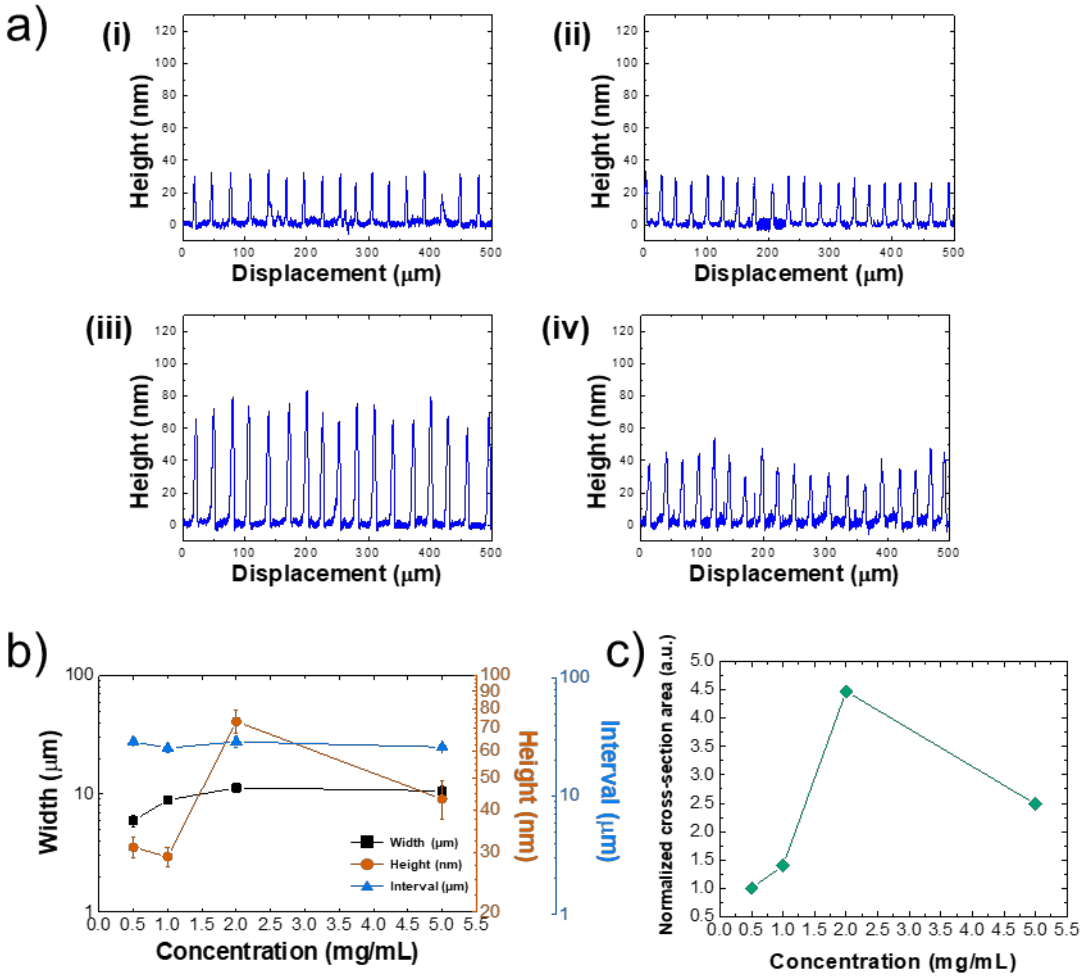

Figure S17. Height profile of P3HT line pattern with different P3HT concentration. (a) Concentration variations: (i) 0.5 mg/mL; (ii) 1.0 mg/mL; (iii) 2.0 mg/mL; (iv) 5.0 mg/mL (50 ºC stage, speed of roller rotation: 1250 rpm, stage speed: 1.0 mm/s). (b) Summary of interval, height, and width of line pattern with different P3HT concentration. (c) Normalized cross-section area of P3HT line pattern with different concentration.